Thermoacoustic Instabilities in Gas Turbines and Rocket Engines: Industry meets Academia
May 30 – June 02, 2016
Munich, Germany
Paper No.: GTRE-010

Bifurcation study of azimuthal bulk flow in annular combustion systems with cylindrical symmetry breaking

Driek Rouwenhorst, Jakob Hermann [1] and Wolfgang Polifke[2]

Abstract

In annular combustion systems, azimuthal thermoacoustic modes can manifest themselves predominantly as traveling or standing waves. Several phenomena can influence the modal behavior of annular thermoacoustics. In monitoring the stability of azimuthal thermoacoustics in industrial installations, a better understanding of the dynamics is required to correctly interpret online measurements. In this work the dynamic solutions of annular combustion systems are investigated, using a low-order analytic model. Heat release fluctuations are considered as a weak source term for a given acoustic eigenmode. The heat release is modeled as a linear feedback to the local acoustics, in which the feedback response is a function of the azimuthal coordinate, causing cylindrical symmetry breaking. A bifurcation map is generated as a function of azimuthal mean flow velocity around the annulus. A bifurcation between solutions fixed by the combustion chamber coordinate system and solutions convected with the azimuthal bulk flow is observed. Due to the interaction with non-uniform thermoacoustic feedback, an azimuthal flow with low Mach number can significantly influence the system stability. At the bifurcation point, the system matrix is defective, which yields unbounded transient growth for vanishing stability.

Keywords

thermoacoustic stability, annular combustor, analytic modeling

Introduction

The risk to encounter thermoacoustic instability in combustion systems increases under lean and flexibly varying operation conditions. A thorough understanding of the thermoacoustic dynamics is required for efficient control or monitoring strategies. In particular the complex dynamics in annular gas turbines has not yet been fully understood. The lack of an acoustic boundary condition in azimuthal direction adds a degree of freedom to the system, allowing for standing waves, traveling waves and combinations thereof. Fundamentally, the two azimuthal waves corresponding to an azimuthal mode number have equal growth rates and form an eigenspace in linear stability analysis. Any breaking of the cylindrical symmetry, either geometric or in the flame response, will lead to split eigenvalues. Considering the acoustics from the fixed coordinate system, an azimuthal flow splits the eigenvalues too.

In this work, the interaction between azimuthal flow and cylindrical symmetry breaking is analyzed analytically. The latter promotes standing wave behavior, whereas the former counteracts the formation of standing wave solutions by rotating the acoustic field with respect to the gas turbine. As both effects are likely to occur to a certain extent in practical annular combustors, their interaction may contain dynamical behavior of interest. The solution regimes resulting from these effects have been recognized in Bauerheim et al. Bauerheim et al. (2014), but the interaction has not been investigated in detail. In the work of Noiray Noiray et al. (2011) the effect of nonlinear and non-uniform heat release response strength is investigated. A full LES-simulation of an annular combustion chamber shows a bulk velocity emerging Wolf et al. (2012), exceeding an azimuthal Mach number of 1% as a result of co-rotating swirl burners.

Azimuthal flow and cylindrical symmetry breaking

In this section it is elaborated how the two phenomena - azimuthal flow and cylindrical symmetry breaking - can arise in annular combustion systems.

Azimuthal flow

In most annular combustion systems, flow around the annulus is restricted in neither the combustion chamber, nor the plenum. In axial direction there is a constant flow of fresh and burnt gases, that can reach high velocities at certain positions. It is to be expected that (depending on the operating conditions) some net momentum transfer in azimuthal direction occurs, for example at the compressor exit in the plenum of a gas turbine, or at the swirl burner in the combustion chamber. Experimental evidence of azimuthal flow, or at least different acoustic propagation velocities in the opposing azimuthal directions, can be found

[1] IfTA GmbH, Germany
[2] Technische Universität München, Germany

Corresponding author:
Driek Rouwenhorst, IfTA Ingenieurbüro für Thermoakustik GmbH Industriestr. 33, 82194, Gröbenzell, Germany.
Email: driek.rouwenhorst@ifta.com

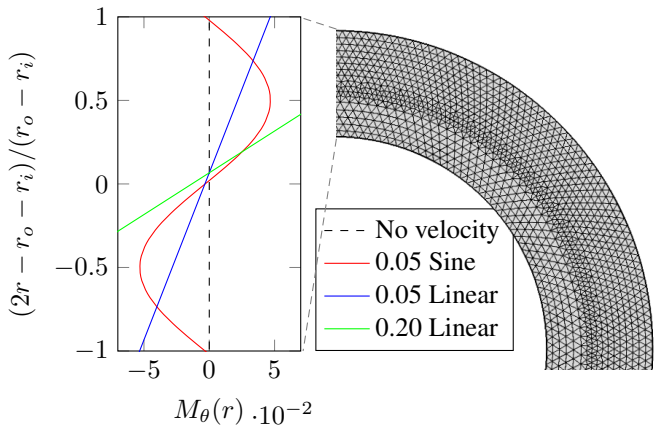

Figure 1. Tested azimuthal velocity profiles as a function of the radius. A quarter of the mesh used for the computation is shown on the right side.

in Worth and Dawson (2013) for varying burner separation distances.

Besides an actual azimuthal bulk flow, another mechanism is investigated here that can cause a difference in effective propagation speed between clockwise and anticlockwise traveling acoustic waves. Such difference in propagation speed is caused by a gradient of azimuthal velocity with respect to the radial coordinate, refracting the acoustic waves. Such shear flow in an annulus refracts waves in one azimuthal direction towards the center of the annulus, whereas the wave in the other direction is constantly refracted towards the outer wall. A radially distributed azimuthal velocity field can be expected in annular combustion systems when co-rotating swirlers are used, see Bourgouin et al. (2013) for the cold flow velocity field downstream of a swirl burner. Strong refraction can also be expected as a result of temperature gradients, however, this will affect the two waves in opposite direction identically.

Table 1. Increment of the eigenfrequencies as a result of azimuthal velocity gradients, with respect to frequency in the quiescent case ω_m. The first two mode orders m are given.

Velocity profile	m	$\omega_{cw}/\omega_m - 1$	$\omega_{acw}/\omega_m - 1$
No velocity	1	0	0
0.05 Sine	1	$-7.3 \cdot 10^{-3}$	$10.7 \cdot 10^{-3}$
0.05 Linear	1	$-8.6 \cdot 10^{-3}$	$11.0 \cdot 10^{-3}$
0.20 Linear	1	$-19.9 \cdot 10^{-3}$	$57.8 \cdot 10^{-3}$
No velocity	2	0	0
0.05 Sine	2	$-6.7 \cdot 10^{-3}$	$10.0 \cdot 10^{-3}$
0.05 Linear	2	$-8.0 \cdot 10^{-3}$	$10.2 \cdot 10^{-3}$
0.20 Linear	2	$-18.5 \cdot 10^{-3}$	$53.9 \cdot 10^{-3}$

To demonstrate eigenvalue splitting as a result of a gradient of azimuthal velocity in radial direction, a 2D annular geometry with a ratio between the outer and inner radius of $r_o/r_i = 1.5$ is considered. Over the width of the annulus azimuthal velocity profiles are prescribed, without bulk flow contribution. A linear and harmonic profile with a peak to peak azimuthal Mach number of $M_{p2p} = 0.1$ are used. Additionally, a linear profile with a peak to peak of $M_{p2p} = 0.4$ is tested. The velocity in the latter case is too high to be expected in practice, but this case can be used for analytical validation as the refraction radius is equal to the radius of the annulus. Acoustic solutions are obtained by solving the Euler equations numerically. A quarter of the mesh is shown in Fig. 1, together with the three velocity profiles. It must be noted that the velocity profiles have a small offset, in order to force the mean flow (integrated in polar coordinates) to be zero.

The influence of the velocity profiles on the eigenfrequencies of azimuthal orders $m = 1$ and $m = 2$ are given in Table 1. The eigenfrequencies ω_{cw} and ω_{acw} correspond to a clockwise and anticlockwise wave respectively. It is concluded that waves that are refracted towards the center of the annulus (which are clockwise waves for the used profiles in Fig. 1), experience a decreased frequency. This can be explained in a loss of the radial wave number. When the refraction radius is equal to the radius of the annulus, plane wave propagation is obtained and the lowest frequency is obtained as the radial wave number is zero. The waves refracted away from the center have a increased frequency. On basis of the analytic acoustic solution in an annulus (Bessel functions), the value for 0.20 Linear should have actually been $\omega_{cw}/\omega_m - 1 = -19.7 \cdot 10^{-3}$. As this investigation is focusing on orders of magnitude, the deviation is considered acceptable. For higher mode orders (shorter wavelengths) the deviation from the analytical solution increases.

For $m = 1$ and a peak to peak azimuthal Mach number of $M_{p2p} = 0.05$, a difference in frequency of almost $0.02\omega_1$ is observed, which can be translated to an "effective azimuthal Mach number" of $M_\theta \approx 0.01$.

This investigation shows that a velocity gradient in the azimuthal flow, can cause a significant split in wave propagation speed in the two directions. In the bifurcation study all possible effects that cause an "effective azimuthal bulk flow" are represented by the azimuthal bulk flow velocity v_θ.

Cylindrical symmetry breaking

For prescribed wavenumbers in the spatial directions, the acoustic field in an annulus is described by two complex amplitudes. In case of cylindrical symmetry (geometry and parameters are invariant under angular rotation), the system manifests a pair of degenerate eigenvalues. Through non-uniformities in azimuthal direction, the eigenvalues can split, i.e. loose the degeneracy. A constriction in an annulus causes two standing wave solutions, with the eigenvalue splitting predominantly resulting in two different eigenfrequencies Choe (1997). Similarly, acoustic sources (or sinks) varying with the azimuth can cause splitting of the growth rates.

A non-uniform flame response to the acoustics of the burners can cause eigenvalue splitting, as the heat release is an acoustic source. The alternating use of two burner types could be applied in an annular combustor as a form of staging, such that a smoother overall flame response is obtained, that is less prone to instabilities Joos et al. (2002). In such case, the chosen burner pattern influences the splitting strength Berenbrink and Hoffmann (2000) and therewith the stability of the system.

Unintended azimuthal non-uniformities are likely to be present in industrial applications. One can think of clogged fuel injection holes, deviations in acoustic impedance of the fuel injections and acoustic reflections from supporting

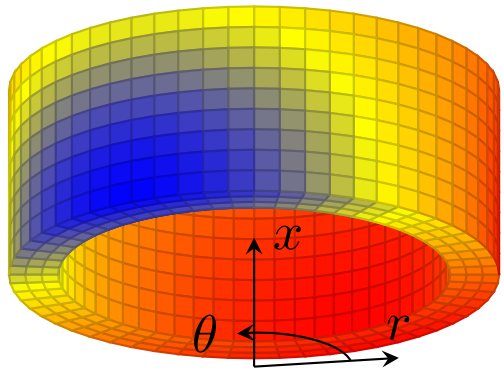

Figure 2. Example of an acoustic field of first azimuthal mode order, which could be described by Eq. (1)

structures, just to name a few. In this work it is implied that the eigenvalue splitting is caused by a non-uniform flame response, but it might as well be of acoustic nature.

Modeling approach

The acoustics is described by a three-dimensional acoustic solution in an annulus, with two azimuthal wave amplitudes as free variables. The acoustic solution is convected passively with an azimuthal bulk flow. Axial flow does not seem to influence the dynamic solution Evesque et al. (2003) and is therefore not considered. As in Noiray et al. (2011), heat release fluctuations are continuously modeled over the azimuth of the annulus, rather than considering discrete burner locations. Local acoustic fluctuations result in heat release fluctuations at the corresponding angular location, through a linear flame response description. The heat release acts as a source to the acoustic pressure fluctuations, described on a Fourier basis over the azimuth.

Linear relations are used, since the dynamic behavior in the stable regime is sought, i.e. before exponential growth and saturation to a limit cycle occurs. It is assumed that the magnitude of combustion noise does not cause a significant nonlinear response. Also, it is assumed that instantaneous growth rates and the angular bulk velocity are small compared to the considered eigenfrequency under all circumstances, such that time scales of amplitude modulations can be separated from the time scale of an acoustic cycle. The resulting system of equations is a state space model with two complex degrees of freedom per degenerate acoustic eigensolution. The dynamic behavior of this system is very suited to be evaluated analytically.

Acoustic field

Thermoacoustics is described by a sum of independent eigenmodes, based on solutions of the acoustic field. Assume that one modal solution of the 3D acoustic pressure field $\hat{p}$ with frequency ω_a is separable in the following way

$$\hat{p}(\tilde{\mathbf{x}}, t) = \psi(x, r)\phi(\tilde{\theta})e^{i\omega_a t} \tag{1}$$

The particle velocity follows directly from the acoustic pressure, according to the acoustic momentum equation. The spatial function $\psi(x, r)$ is assumed to be known, fulfilling the wave equation for given longitudinal and radial boundary conditions in the annular combustion chamber. Azimuthal dependency $\phi(\tilde{\theta})$ is not fully determined by boundary conditions, as no boundary is present in this direction.

$$\phi(\tilde{\theta}) = \hat{F}e^{-im\theta} + \hat{G}e^{im\tilde{\theta}} = \mathbf{b}^T\mathbf{z} \tag{2}$$

In which the vector $\mathbf{z} = [\hat{F}\ \hat{G}]^T$ contains the two Riemann invariants as free acoustic parameters, while $\mathbf{b} = [e^{-im\tilde{\theta}}\ e^{im\tilde{\theta}}]^T$ contains their respective azimuthal basis functions. These basis functions fulfill the wave equation harmonically for a domain with uniform acoustic properties in azimuthal direction, for positive definite azimuthal mode number m. The azimuthal coordinate $\tilde{\theta}$ is defined relative to the azimuthal bulk velocity component v_θ, since the acoustics are passively convected by the flow field. In the coordinate system of the combustor, the acoustics is considered relative to the azimuthal bulk flow v_θ by substitution of $\tilde{\theta} = \theta - v_\theta t$.

Equation (1) is the fundamental solution of a 3D acoustic field in a cylindrically symmetric geometry with azimuthal bulk flow. Choosing the amplitudes $\hat{F}$ and $\hat{G}$, standing, traveling and mixed solutions can be constructed. The two amplitudes and complex angles give four free variables.

Thermoacoustic feedback

Weak thermoacoustic feedback is added to the acoustic mode, to find the combined dynamics. A relatively low acoustic damping ratio $\zeta \ll 1$ is assumed such that the acoustics dominate the resulting modal eigenfrequency. The thermoacoustic feedback is considered as small linear perturbations to the acoustic field, allowing separation of the acoustic time scale and the time scale of the thermoacoustic coupling. Dynamics dominated by the time scale of the combustion, such as intrinsic thermoacoustic instability Emmert et al. (2015), are not considered.

The Rayleigh criterion states that acoustic energy is generated when heat release fluctuations $\dot{Q}$ are in phase with the pressure fluctuations. The growth of the acoustic mode in consideration is obtained by integrating over the volume in which the heat is released. Using $\star$ to denote the complex conjugate, the following equation can be derived (see Appendix A).

$$\frac{\mathrm{d}\mathbf{z}}{\mathrm{d}t} = \kappa \oint \mathbf{b}^\star \dot{Q}\, \mathrm{d}\theta - v_\theta \left(\mathbf{b}^\star \cdot \mathbf{z} \cdot \frac{\mathrm{d}\mathbf{b}}{\mathrm{d}\tilde{\theta}} \right) \tag{3}$$

The proportionality constant κ is related to the volume of the acoustic domain and the ratio of specific heats. Prevailing methods for the modeling of heat release fluctuations assume a linear response to the acoustics at the burners, for low perturbation amplitudes. Examples are the flame transfer function and the sensitive time lag model. A general linear heat release response to the two acoustic waves could be written as

$$\kappa\dot{Q}(\theta) = \mathbf{b}^T \left(\left[\hat{C}^F(\theta) \quad \hat{C}^G(\theta) \right]^T \cdot \mathbf{z} \right) \tag{4}$$

In which the complex-valued coefficients $\hat{C}^F$ and $\hat{C}^G$ represent the amplitude and phase of the heat release response to the respective waves in $\mathbf{q}$. These response coefficients are a function of the azimuth in case of non-uniform heat release, causing cylindrical symmetry breaking. Apart from the heat release, the coefficients can also

include acoustic effects, such as attenuation and reflections. Combining the linear heat release response in Eq. (4) with the acoustic modal growth Eq. (3) yields the thermoacoustic system of ordinary differential equations.

$$\frac{\mathrm{d}\mathbf{z}}{\mathrm{d}t} = \oint \begin{bmatrix} \hat{C}^F + imv_\theta & \hat{C}^G e^{2im\theta} \\ \hat{C}^F e^{-2im\theta} & \hat{C}^G - imv_\theta \end{bmatrix} \mathrm{d}\theta\, \mathbf{z} \tag{5}$$

From the integration of the system matrix over the azimuthal coordinate, it can be directly deduced that the diagonal only depends on the average of $\hat{C}^F$ and $\hat{C}^G$. On the other hand, the antidiagonal is only sensitive to coefficient $2m$ of the azimuthal Fourier decomposition of $\hat{C}^F$ and $\hat{C}^G$. Describing the coupling coefficients $\hat{C}$ as Fourier series over the azimuth therefore allows to perform the integration directly.

$$\hat{C}(\theta) = \sum_{k=-\infty}^{\infty} \hat{c}_k e^{ik\theta} \tag{6}$$

The general description of the thermoacoustic dynamics is reduced to a complex second order system of ODE's per acoustic eigenvalue pair. In the work of Bauerheim Bauerheim et al. (2014) this solution structure was also found, modeling the heat release with an $n-\tau$ model.

$$\frac{\mathrm{d}\mathbf{z}}{\mathrm{d}t} = \begin{bmatrix} \hat{c}_0^F + imv_\theta & \hat{c}_{-2m}^G \\ \hat{c}_{2m}^F & \hat{c}_0^G - imv_\theta \end{bmatrix} \mathbf{z} \tag{7}$$

The coupling coefficients $\hat{c}_k$ can be a function of the frequency to be solved for, for example in the case of an $n-\tau$ model, in which the phase linearly decreases with frequency.

$$\dot{\mathbf{z}} = \mathrm{M}(\omega)\mathbf{z} \tag{8}$$

The system matrix M describes the coupling between the two (complex) acoustic degrees of freedom, including thermoacoustic interaction. Under additional flame response assumptions, the coupling coefficients can be specified in more detail.

Solution strategy

Equation (8) is valid when the model parameters (the coupling coefficients and radial bulk velocity) are very small compared to the acoustic eigenfrequency and the dominating azimuthal acoustics behave linearly. In order to come to an analytic eigensolution of the system, the system matrix must be independent of the frequency. When this is not the case, the characteristic equation of $M(\omega)$ is a transcendent equation for the eigenvalues (or complex frequency) that must be solved numerically. For small frequency dependency, however, a linearized eigensolution will yield accurate solutions.

The imaginary part of an eigenvalue of the system matrix M represents the frequency deviation $\Delta\omega$ from the acoustic eigenfrequency ω_a. When the coefficients $\hat{C}(\omega)$ hardly change on the interval $[\omega_a - \Delta\omega < \omega < \omega_a + \Delta\omega]$, the dependency can be neglected.

$$\left| \frac{\Delta\omega}{\hat{C}} \frac{\mathrm{d}\hat{C}}{\mathrm{d}\omega}|_{\omega_a} \right| \ll 1 \tag{9}$$

As $\Delta\omega$ is of the order of $|\hat{C}|$, it can just be stated that the derivative of the coupling parameters with respect to the frequency should be very small. Weak thermoacoustic feedback - as stated in the previous subsection - should be interpreted as $\mathrm{d}\hat{C}/\mathrm{d}\omega \ll 1$, such that an accurate analytical solution can be found.

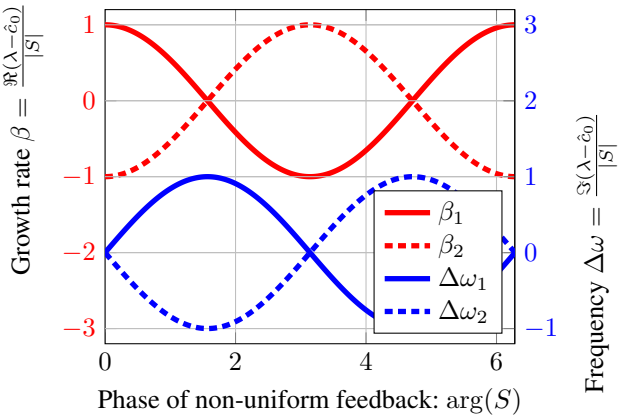

Figure 3. Effect of the phase of the non-uniform feedback $\arg(S)$ on the eigenvalues of the thermoacoustic system, without azimuthal bulk velocity v_θ. Normalization by the cylindrical asymmetry strength $|S|$

Results: Feedback based on axial velocity

Heat release fluctuations, due to vortical structures and equivalence ratio modulations, are usually attributed to the axial particle velocity, see for example Paschereit and Polifke (1998). When axial particle velocity is held responsible for the fluctuating heat release, the thermoacoustic system is a function of the pressure fluctuations and independent of the azimuthal particle velocity. Also assuming coupling constants that are (locally) independent of the frequency ($\frac{\mathrm{d}\hat{C}}{\mathrm{d}\omega} = 0$), the coupling parameters are equal ($\hat{C}^F = \hat{C}^G = \hat{C}$). These assumptions are made only to obtain a compact analytic eigensolution.

$$\frac{\mathrm{d}\mathbf{z}}{\mathrm{d}t} = \begin{bmatrix} \hat{c}_0 + imv_\theta & \hat{c}_{-2m} \\ \hat{c}_{2m} & \hat{c}_0 - imv_\theta \end{bmatrix} \mathbf{z} \tag{10}$$

This reduced system of differential equations, as a function of mv_θ and the Fourier components of $\hat{C}(\theta)$, is used as the starting point of the analytic parameter study performed in this work. The eigensolution is:

$$\lambda_{1,2} = \hat{c}_0 \pm \sqrt{\hat{c}_{2m}\hat{c}_{-2m} - m^2 v_\theta^2} \tag{11}$$

In Eq. (11) it is visible how azimuthally varying heat release characteristics and azimuthal velocity split the eigenvalues $\lambda_{1,2}$ of the thermoacoustic system. Also the ratios of $\hat{F}$ and $\hat{G}$ corresponding to the eigenvectors are readily obtained

$$\nu_{1,2} = \frac{imv_\theta}{\hat{c}_{2m}} \pm \frac{1}{\hat{c}_{2m}} \sqrt{\hat{c}_{2m}\hat{c}_{-2m} - m^2 v_\theta^2} \tag{12}$$

The influence of the model parameters on the acoustic eigensolution and their interaction will now be explained in detail. From the eigensolution it can be seen that the interacting parameter groups are mv_θ, i.e. radial velocity with respect to the azimuthal wave length, and the cylindrical

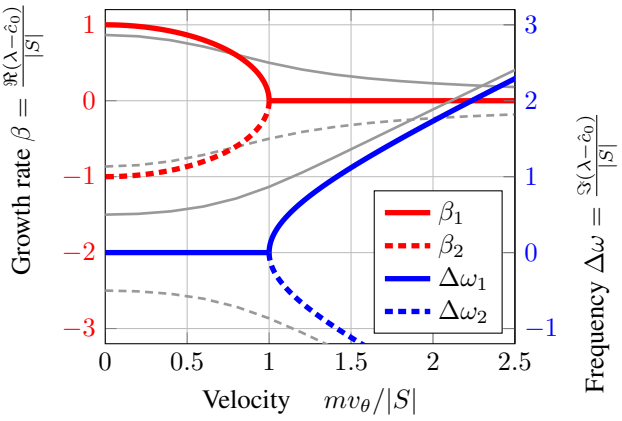

Figure 4. Normalized effect of the interaction between mv_θ and cylindrical symmetry breaking S on the eigenvalues of the thermoacoustic system, with $\arg(S) = 0$. In gray thin lines the result for $\arg(S) = \pi/6$

symmetry breaking

$$S = \sqrt{\hat{c}_{2m}\hat{c}_{-2m}} \tag{13}$$

Uniform feedback $\hat{c}_0$ only ($mv_\theta = S = 0$)

Without azimuthal non-uniformity of the thermoacoustic feedback response and no bulk velocity, the eigenvalues of the system are simply given by the constant feedback strength $\hat{c}_0$ on the diagonal of the system matrix. With repeated eigenvalues, the system is degenerate, with solutions in the eigenspace spanned by $\hat{F}$ and $\hat{G}$. This means that linear combination of the two waves is an eigensolution, covering standing, traveling and mixed modes. The growth rate and frequency difference as a function of $\arg\hat{c}_0$ are the cosine and sine function respectively. With $\hat{c}_0$ located on the matrix diagonal, it does not interact with the other system parameters.

Azimuthal flow mv_θ, with $S = 0$

Only considering azimuthal bulk flow still yields the trivial solution, rotating with the mean flow. The rotation is visible in the imaginary split eigenvalues by $\pm imv_\theta$ for $\hat{F}$ and $\hat{G}$ respectively.

Cylindrical symmetry breaking S, with $mv_\theta = 0$

A pair of standing waves evolve as a result of non-uniform feedback, with eigenvalues that are split by S, as defined in Eq. (13). When S has a real contribution, a saddle point is formed by two orthogonal standing waves, one with positive and one with negative feedback. It can be comprehended that the azimuthal order $2m$ of $\hat{C}(\theta)$ causes this splitting, as it excites the $2m$ anti-nodes of these standing waves respectively. In Fig. 3 the growth rate and frequency are shown as a function of $\arg(S)$, which is the phase between the acoustic pressure and heat release in the considered case where the heat release is proportional to the axial particle velocity. This phase is directly related to the phase of a flame transfer function, describing the heat release.

Interaction between mv_θ and S

As both mv_θ and S appear in the root in the eigensolution equations (11,12), some interaction takes place, shaping the modal solutions. What the eigenmodes look like is not directly clear from the analytic expressions. The interaction in this intermediate regime can be understood qualitatively as follows; the azimuthal feedback non-uniformity tries to develop a standing wave solution, but the bulk velocity constantly rotates the acoustic field away from its standing wave angle. Two new equilibria will therefore evolve, given by the full eigensolution. The interaction is most pronounced when the two effects are of similar magnitude; $|S| \approx |mv_\theta|$. In the regime where $|mv_\theta/S| \ll 1$, solutions are predominantly standing waves, whereas $|mv_\theta/S| \gg 1$ can be characterized as traveling waves.

The velocity term can cancel out the eigenvalue splitting as a result of the heat release non-uniformity. The important observation is that only limited azimuthal velocity is required for noticeable changes for the stability analysis. Instability is most likely to occur in very underdamped (thermo)acoustic eigenmodes, say with a damping ratio of the order $\zeta = -\Re(\lambda_{min})/2/\omega_a = \mathcal{O}(10^{-2})$. Azimuthal velocity can potentially change the stability with strength mv_θ, therefore azimuthal Mach numbers of the same order $M_\theta = \mathcal{O}(10^{-2})$, are already relevant in the presence of cylindrical symmetry breaking.

Bifurcation point

The case where $\hat{c}_{2m} = \hat{c}^*_{-2m}$ is of most interest, because the feedback contributes optimally to the real part of the eigenvalues and thus to the system stability. The symmetry breaking S is real and the feedback phase is constant around the azimuth. The bifurcation diagram with mv_θ the bifurcation parameter, forms a unit circle and unit parabola for the growth rate and frequency difference respectively, when normalized by $|S|$ (see Fig. 4). Without azimuthal velocity, two standing wave solutions in orthogonal orientations are found, with pure positive and negative feedback. In a phase plot this solution is represented by a saddle point, as shown in the first plot of Fig. 5. As a mean flow is introduced the growth rate splitting decreases and simultaneously the eigenvectors lose their mutual orthogonality. A bifurcation point at $|mv_\theta| = S$ emerges as the discriminant in the root of the dynamical system crosses zero. At this point the two eigenvectors coincide, as Fig. 5 suggests. In other words, the eigenvectors are linearly dependent and the system matrix is defective. For comparison, a case with complex S is shown in Fig. 4 (gray lines), that does not cross the bifurcation point. In that case, the feedback partially acts on the frequency, preventing the discriminant in the eigensolution (Eqs. (11,12)) to become zero.

The bifurcation point as shown in Fig. 4 can be dangerous during the operation of an annular combustion system. As the bifurcation parameter varies a little, the stability abruptly changes at the bifurcation point.

Non-normal growth

In case of non-normality - coinciding eigenvectors in special - perturbations to the system can experience transient

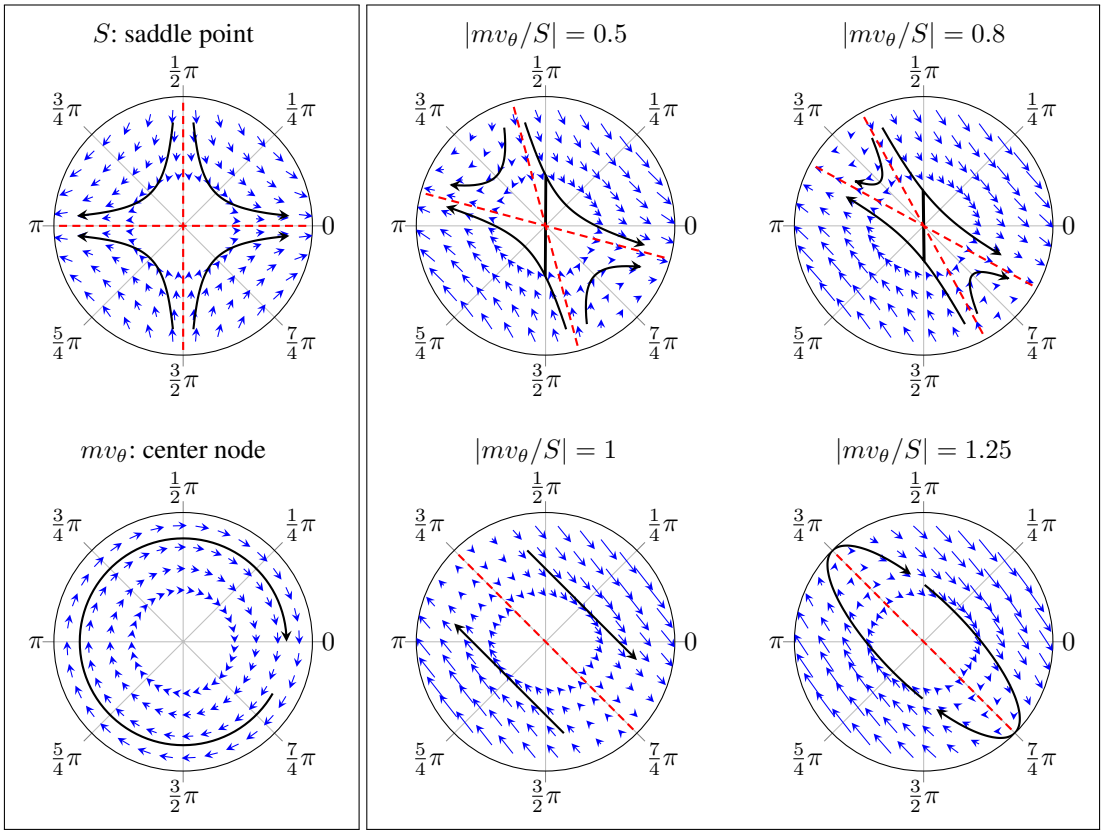

Figure 5. Phase plots of the thermoacoustic system for real azimuthal symmetry breaking S, in the vector space of two orthogonal standing wave angles per azimuthal wavelength: $m\theta$. All phase trajectories represent the dynamics of standing waves. A real azimuthal asymmetry S results in a saddle point, with an instable standing wave at the orientation $m\theta = 0$ and a stable standing wave at $m\theta = \pi/2$. Increasingly adding azimuthal velocity - a center node - brings the eigenvectors together, shown as red dashed lines. In the bifurcation point ($|mv_\theta| = S$), a neutrally stable improper node found, with coinciding eigenvectors. For higher velocities the solutions are convected by the flow and are no longer pure standing waves. A contribution of $\hat{c}_0$ could be included by superposing a star node, influencing the overall stability.

amplification. When the system has a nonlinear response to the amplitude, an instability can be triggered in the linearly stable regime. Non-normal growth has been studied in thermoacoustic systems, based on modeling Juniper (2010) as well as experiments Kim and Hochgreb (2012). In this section non-normal growth in annular combustion systems is demonstrated in the bifurcation point of the model system. Due to the annular geometry, the amplitude amplification can occur at a single mode order, revealing an insightful physical mechanism behind the transient growth.

The dynamic solution of the defective system matrix takes the form

$$\mathbf{z}(t) = 2S\left(Ate^{\hat{c}_0 t} + Be^{\hat{c}_0 t}\right)\mathrm{v} + Ae^{\hat{c}_0 t}\mathrm{w} \qquad (14)$$

Where v is the (repeated) eigenvector, while w is chosen as the standing wave orthogonal to v. Amplitudes A and B follow from initial conditions.

The term $Ate^{\hat{c}_0 t}$ causes the transient behavior before the exponential decay sets in. Transient growth can occur only when the system would have been unstable in one orientation (saddle point), if there were no azimuthal bulk flow. From the solution in Eq. (14), the maximum transient growth can be obtained analytically (see Appendix). For $\Re(\hat{c}_0)^2 \ll S^2$, the time after which the maximum amplification occurs is approximately $t_{\max} = -1/\Re(\hat{c}_0)$, reaching a maximum possible amplification ratio of about

$$\frac{|\mathbf{z}(t)|}{|\mathbf{z}_0|} = \frac{-2S}{\Re(\hat{c}_0)e} \qquad (15)$$

The transient growth is demonstrated for $S = mv_\theta = 10s^{-1}$ and an overall thermoacoustic decay of $\Re(\hat{c}_0) = -2s^{-1}$. The phase plot of the dynamic system is shown in the top of Fig. 6. The two thick green solutions experience the maximum possible transient growth, starting on the gray unit circle. In the plot below this transient growth of the amplitude is shown as a function of time. A maximum amplitude amplification of 3.7 is reached, as estimated by Eq. (15), which is equivalent to an amplification factor of over 13 for the acoustic energy.

Alternatively the maximum amplification and their corresponding initial conditions can be found computationally, as for example in Nagaraja et al. (2009). Using this approach the same results have been found (not shown). For this specific low-dimensional model, the amplification can be computed analytically in the bifurcation point. This way it is found that theoretically, infinite transient growth can be obtained, for nonzero splitting strength and vanishing stability. Refer to $|mv_\theta/S| = 1$ in Fig. 5, where a perturbation away from the eigenvector pair linearly grows to infinity, even though the system is marginally stable.

With help of the phase plot representations, the transient behavior of this system can be easily understood physically.

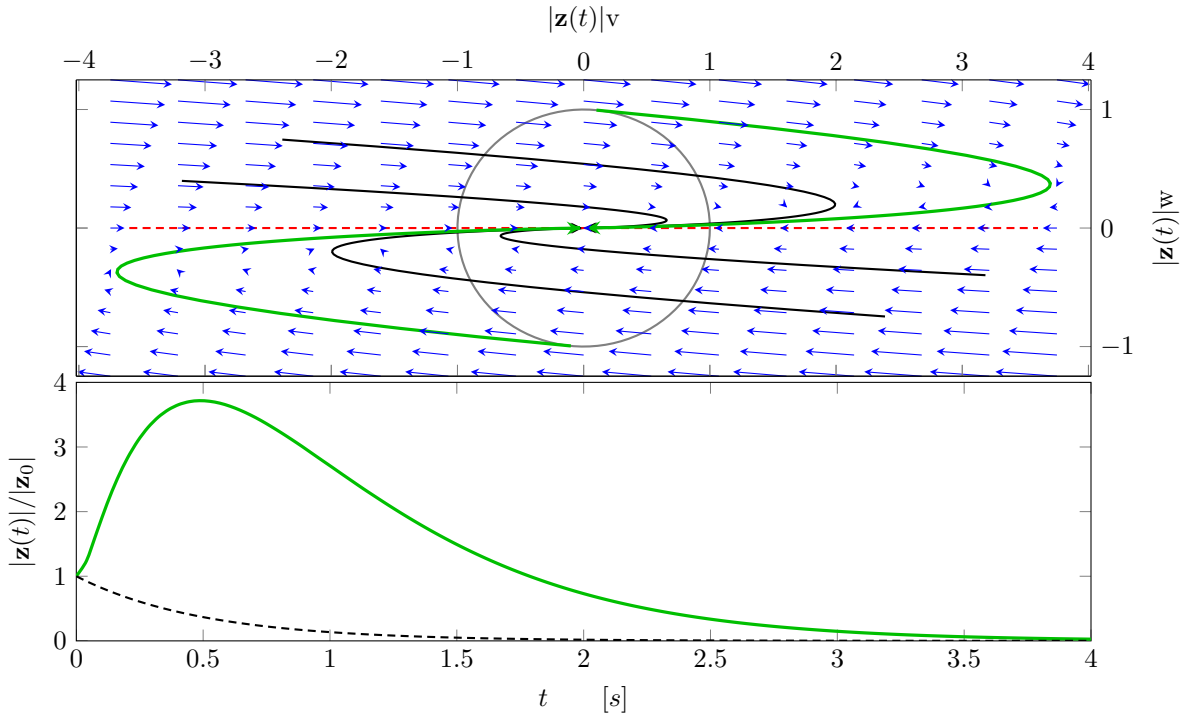

Figure 6. Transient growth of the acoustic amplitude in the bifurcation point of the system, with $S = mv_\theta = 10s^{-1}$ and $\lambda = \Re(\hat{c}_0) = -2s^{-1}$, starting from the initial conditions that lead to the maximum transient growth. Above the evolution in the phase plot (eigenvector aligned with the x-axis) shows the rotation of the acoustic field. Below, the growth is plotted as a function of time, compared to the case of normal decay (dashed line). The maximum growth amplification is very accurately approximated by Eq. (15)

A perturbation in an unstable orientation of the symmetry breaking will initialize exponential growth. In the phase plot of Fig. 6, these orientations are located in quadrant 1 (positive-positive) and quadrant 3 (negative-negative). The azimuthal flow then convects the growing amplitude around the circumference, towards the stable orientation of the saddle node. The growth will come to a halt and the perturbation will eventually converge to the least stable eigenmode and decay accordingly.

Amplitude statistics under stochastic excitation

The maximum transient amplification shows what amplitude can be reached for an optimized initial condition. More interesting is what effect the non-normality of the system has on the characteristics under constant stochastic forcing. To investigate this, the system of equations (Eq. (10)) is integrated numerically with white noise, using the Euler-Mayurama scheme. The system is compared to the uncoupled, degenerate case (uniform heat release response) with the same set of eigenvalues $\Re(\lambda_{1,2}) = \Re(\hat{c}_0) = -2$. Part of the two time series, that were subjected to the same excitation noise, are shown in Fig. 7. The average amplitude (RMS) of the non-normal system is found to be 5 times higher (25 times for the acoustic energy) than the degenerate system, which is higher than the maximum possible non-normal growth ratio. This result suggests it is more interesting to look at the integral of the amplitude over time for all initial conditions, rather than looking at the maximum possible amplification.

The probability density function of the euclidean norm of four independent, normal distributed variables (two complex amplitudes) is given by the χ_4 distribution. The histogram of the bottom time series in Fig. 7 shows that the χ_4 distribution accurately describes the likeliness of the amplitudes found for the uncoupled thermoacoustic system. For the non-normal system matrix, however, the amplitude distribution is much better described by the χ_2 distribution, i.e a process with only two independent variables. This result can be explained by the strong coupling of the waves (caused by the anti-diagonal in the system matrix, Eq. (10)), predominantly yielding standing waves under a preferred angular orientation. The latter distribution has a higher kurtosis than the former, which means that the observed peaks in the time series are relatively high with respect to the mean amplitude. As a last note, the autocorrelation of the absolute acoustic amplitude of the defective system matrix does not decay exponentially and decays slower than one might expect from the eigenvalue pair.

Conclusion

An annular thermoacoustic system with both azimuthal bulk flow and non-uniform response can show very interesting dynamics, even under linear assumptions. As the damping ratio is typically very low, it is found that small azimuthal Mach numbers can be relevant for the thermoacoustic stability through the interaction with azimuthal non-uniformities. Solving the acoustic field numerically, it is demonstrated that a velocity gradient in the azimuthal flow acts as an ”effective azimuthal bulk flow”. The effective azimuthal flow in the annulus can stabilize standing wave solutions that would otherwise be unstable as a result of eigenvalue splitting. The other way round, a loss of bulk

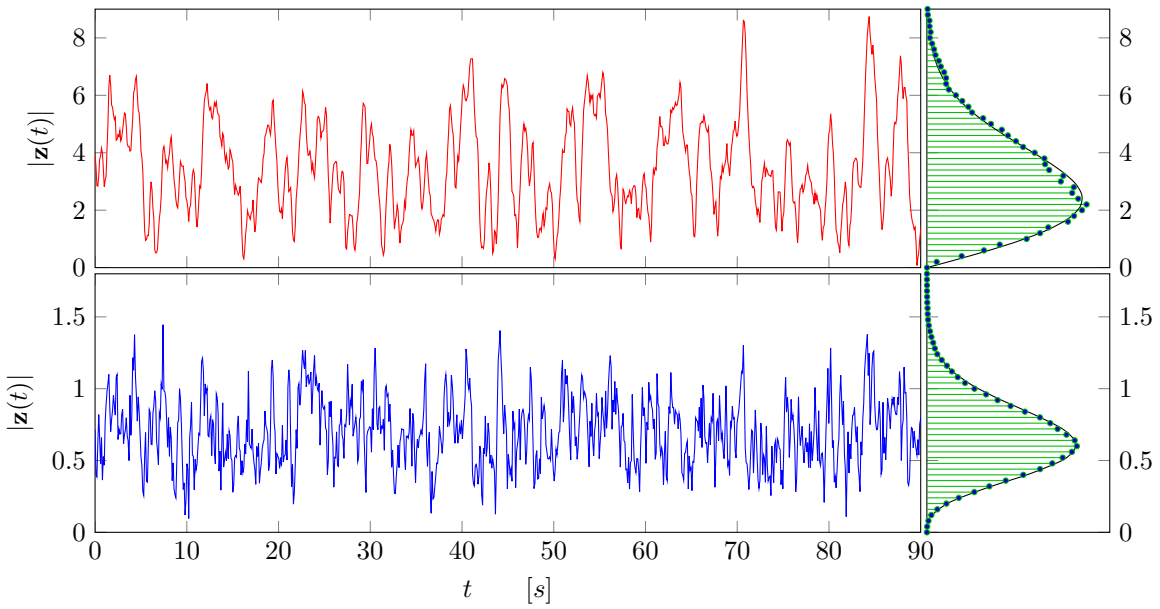

Figure 7. Time series of stochastically forced systems, with eigenvalues $\lambda_{1,2} = -2s^{-1}$. Above: Bifurcation point, Below: Degenerate case (uncoupled). The RMS value of the non-normal system is 5 times higher compared to the degenerate case, both under unit forcing strength. Note the difference in amplitude histograms (based on 14 minutes) on the right, compared to χ_2 and χ_4 distributions respectively

flow can cause a sudden decrease of thermoacoustic stability. As the azimuthal flow follows from operating conditions in some non-trivial way, instability can occur unexpectedly. Coupling between the acoustic field and the azimuthal flow field could be an important nonlinear phenomenon in thermoacoustics of annular gas turbines.

The type of eigenmode solution depends on the ratio between the azimuthal flow velocity per wavelength and the cylindrical asymmetry. When their strengths are of the same order of magnitude, both phenomena have to be regarded in the stability analysis of annular thermoacoustic systems. When the ratio is close to one, the system can behave in a strongly non-normal manner. A bifurcation point exists in which the system matrix is defective. It is shown analytically that the maximum transient growth in this point goes to infinity for vanishing system stability.

The defective system can yield significantly higher amplitudes under stochastic forcing, compared to the degenerate counterpart with equal eigenvalues. This effective amplification under random excitation is considered more relevant than the maximum possible transient amplification ratio. Also, the statistical moments of the acoustic amplitude change as a result of the linear coupling between the waves. The increased peakedness of the amplitude should not be mistaken with intermittency due to nonlinearities.

Acknowledgment

The authors express their gratitude to Max Meindl for numerically solving the acoustic Euler equations.

The presented work is part of the Marie Curie Initial Training Network Thermo-acoustic and aero-acoustic nonlinearities in green combustors with orifice structures (TANGO). We gratefully acknowledge the financial support from the European Commission under call FP7-PEOPLE-ITN-2012.

References

Bauerheim M, Salas P, Nicoud F and Poinsot T (2014) Symmetry breaking of azimuthal thermo-acoustic modes in annular cavities: a theoretical study. *Journal of Fluid Mechanics* 760: 431–465. DOI:10.1017/jfm.2014.578.

Berenbrink P and Hoffmann S (2000) Suppression of Dynamic Combustion Instabilities by Passive and Active Means. In: *Int'l Gas Turbine and Aeroengine Congress & Exposition, rmASME paper*, 2000-GT-0079. Munich, Germany: ASME, pp. 7–7.

Bourgouin JF, Durox D, Schuller T, Beaunier J and Candel S (2013) Ignition dynamics of an annular combustor equipped with multiple swirling injectors. *Combustion and Flame* 160(8): 1398–1413. DOI:10.1016/j.combustflame.2013.02.014.

Choe SY (1997) *Investigation of a Constricted Annular Acoustic Resonator*. Master thesis, Naval Postgraduate School, Monterey, California.

Emmert T, Bomberg S and Polifke W (2015) Intrinsic Thermoacoustic Instability of Premixed Flames. *Combustion and Flame* 162(1): 75–85. DOI:10.1016/j.combustflame.2014.06.008.

Evesque S, Polifke W and Pankiewitz C (2003) Spinning and Azimuthally Standing Acoustic Modes in Annular Combustors. In: *Proc. 9th AIAA/CEAS Aeroacoustics Conf., Paper AIAA 2003-3182, 12–14 May 2003, Hilton Head, South Carolina*, AIAA 2003-3182. Hilton Head, S.C., U.S.A.

Joos F, Polifke W and Ni A (2002) Combustion device for generating hot gases. U.S. Classification 60/725, 60/746; International Classification F23R3/30, F23R3/16, F23R3/12, F23R3/28; Cooperative Classification F23R2900/00016, F23R2900/00014, F23D2210/00, F23C2900/07002, F23R3/286; European Classification F23R3/28D.

Juniper M (2010) Triggering in the horizontal Rijke tube: non-normality, transient growth and bypass transition. *Journal of*

Fluid Mechanics : 1–37.

Kim KT and Hochgreb S (2012) Measurements of triggering and transient growth in a model lean-premixed gas turbine combustor. *Combustion and Flame* 159(3): 1215–1227.

Nagaraja S, Kedia K and Sujith RI (2009) Characterizing Energy Growth during Combustion Instabilities: Singularvalues or Eigenvalues? *Proc. Comb. Inst.* 32(1): 2933–2940.

Noiray N, Bothien M and Schuermans B (2011) Investigation of azimuthal staging concepts in annular gas turbines. *Combustion Theory and Modelling* 15(5): 585–606. DOI: 10.1080/13647830.2011.552636.

Paschereit CO and Polifke W (1998) Investigation of the Thermo-Acoustic Characteristics of a Lean Premixed Gas Turbine Burner. In: *Int'l Gas Turbine and Aeroengine Congress & Exposition*, ASME 98-GT-582. Stockholm, Sweden.

Wolf P, Staffelbach G, Gicquel LYM, Müller JD and Poinsot T (2012) Acoustic and Large Eddy Simulation studies of azimuthal modes in annular combustion chambers. *Combustion and Flame* 159(11): 3398–3413. DOI:10.1016/j.combustflame.2012.06.016.

Worth NA and Dawson JR (2013) Modal dynamics of self-excited azimuthal instabilities in an annular combustion chamber. *Combustion and Flame* 160(11): 2476–2489.

Appendix A

Derivation of Eq. (3): The Rayleigh criterion can be written as

$$\frac{1}{\gamma-1}\frac{\mathrm{D}}{\mathrm{D}t}(\hat{p}^\star\hat{p}) = \dot{Q}\hat{p}^\star + \dot{Q}^\star\hat{p} \tag{A-1}$$

Regarding the slow azimuthal dynamics

$$\frac{1}{\gamma-1}\frac{\mathrm{D}}{\mathrm{D}t}(\phi^\star\phi) = \dot{Q}\phi^\star + \dot{Q}^\star\phi \tag{A-2}$$

Seeking the complex growth of ϕ as a function of the heat release $\dot{Q}$, we can keep the following part

$$\phi^\star\frac{\mathrm{D}\phi}{\mathrm{D}t} = (\gamma-1)\dot{Q}\phi^\star \tag{A-3}$$

The equation has to hold for both amplitudes in $\mathbf{z}$ independently as the basis functions are orthogonal, so we can write

$$\frac{\mathrm{D}\mathbf{b}\cdot\mathbf{z}}{\mathrm{D}t} = (\gamma-1)\dot{Q} \tag{A-4}$$

writing out the total derivative

$$\mathbf{b}\cdot\frac{\mathrm{d}\mathbf{z}}{\mathrm{d}t} + v_\theta\left(\mathbf{z}\cdot\frac{\mathrm{d}\mathbf{b}}{\mathrm{d}\tilde{\theta}}\right) = (\gamma-1)\dot{Q} \tag{A-5}$$

to retrieve the effect on $\mathbf{z}$

$$\frac{\mathrm{d}\mathbf{z}}{\mathrm{d}t} = (\gamma-1)\mathbf{b}^\star\dot{Q} - v_\theta\left(\mathbf{b}^\star\cdot\mathbf{z}\cdot\frac{\mathrm{d}\mathbf{b}}{\mathrm{d}\tilde{\theta}}\right) \tag{A-6}$$

The average effect over the volume V can be written as

$$\frac{\mathrm{d}\mathbf{z}}{\mathrm{d}t} = (\gamma-1)V\oint\mathbf{b}^\star\dot{Q}\mathrm{d}\theta - v_\theta\left(\mathbf{b}^\star\cdot\mathbf{z}\cdot\frac{\mathrm{d}\mathbf{b}}{\mathrm{d}\tilde{\theta}}\right) \tag{A-7}$$

because the right-most term is not a function of θ. The volume and ratio of specific heats are combined in a single proportionality constant: $\kappa = (\gamma-1)V$

$$\frac{\mathrm{d}\mathbf{z}}{\mathrm{d}t} = \kappa\oint\mathbf{b}^\star\dot{Q}\mathrm{d}\theta - v_\theta\left(\mathbf{b}^\star\cdot\mathbf{z}\cdot\frac{\mathrm{d}\mathbf{b}}{\mathrm{d}\tilde{\theta}}\right) \tag{A-8}$$

Appendix B

Derivation of Eq. (15): We have the solution in terms of two standing waves (Eq. (14))

$$\mathbf{z}(t) = 2S\left(Ate^{\hat{c}_0 t} + Be^{\hat{c}_0 t}\right)\mathrm{v} + Ae^{\hat{c}_0 t}\mathrm{w} \tag{B-1}$$

A solution that starts on a unit circle and reaches the maximum, will start tangential to the unit circle and then grow. This means the first derivative of the acoustic energy is zero (and the second positive). The acoustic energy is

$$|\mathbf{z}^2(t)| = \left(4S^2(At+B)(A^\star t+B^\star) + AA^\star\right)e^{2\Re(\hat{c}_0)t} \tag{B-2}$$

We know that traveling waves decay with $-\Re\lambda$ without growing transiently (on a time scale longer than a cycle). Therefore any traveling energy content would reduce the transient growth. For this reason, we reduce our search to real values for A and B. Derivative at $t=0$, starting on the unit circle: $A^2+4S^2B^2=1$

$$|\mathbf{z}^2|'_{t=0} = 4ABS^2 + \Re(\hat{c}_0) = 0 \tag{B-3}$$

Solutions for A and B are

$$A = \pm\sqrt{\frac{1}{2}\pm\frac{1}{2}\sqrt{1-\frac{\Re(\hat{c}_0)^2}{S}}} \tag{B-4}$$

$$B = \frac{\sqrt{1-A^2}}{2S} = \pm\sqrt{\frac{1}{8S^2}\mp\frac{1}{8S^2}\sqrt{1-\frac{\Re(\hat{c}_0)^2}{S^2}}} \tag{B-5}$$

One of the (positive and negative) solution pairs are the initial condition for maximum growth, whereas the other pair points to the conditions where the maximum amplitude is located. This can be deduced by looking at the second derivative of the acoustic energy. Inserting the found initial amplitudes in the derivative of acoustic energy, the time to the maximum amplitude can be solved for

$$\frac{1}{2}|\mathbf{z}^2(t)|'e^{-2\Re(\hat{c}_0)t} = 4S^2(A^2t(\Re(\hat{c}_0)t+1) + AB(2\Re(\hat{c}_0)t+1)) + \Re(\hat{c}_0) \tag{B-6}$$

Solving the polynomial for the time t, the time t_{max} is found at which the maximum amplitude is reached

$$t_{max} = \frac{-1}{\Re(\hat{c}_0)}\sqrt{1-\frac{\Re(\hat{c}_0)^2}{S^2}} \tag{B-7}$$

Backsubstitution of t_{max} and amplitudes A and B in Eq. (B-2) yield the maximum amplitude growth, given by

$$\left|\frac{\mathbf{z}}{\mathbf{z_0}}\right|_{max} = \frac{-\Re(\hat{c}_0)}{S}\frac{e^{-\sqrt{1-\frac{\Re(\hat{c}_0)^2}{S^2}}}}{1-\sqrt{1-\frac{\Re(\hat{c}_0)^2}{S^2}}} \tag{B-8}$$

Clearly for $S^2 = \hat{c}_{2m}\hat{c}_{-2m} \gg \Re(\hat{c}_0)^2$ this can be simplified to

$$\left|\frac{\mathbf{z}}{\mathbf{z_0}}\right|_{max} = \frac{-\Re(\hat{c}_0)}{eS}\frac{1}{\frac{\Re(\hat{c}_0)^2}{2S^2}} = \frac{-2S}{\Re(\hat{c}_0)e} \tag{B-9}$$